Using EO-1 Hyperion to Simulate HyspIRI Products for a Coniferous Forest: the Fraction of PAR Absorbed by Chlorophyll ($fAPAR_{chl}$) and Leaf Water Content (LWC)

Qingyuan Zhang[a,b], Elizabeth M. Middleton[b], Bo-Cai Gao[c], Yen-Ben Cheng[d,b]

[a]Goddard Earth Sciences Technology and Research (GESTAR), Universities Space Research Association (USRA), Columbia, MD 21044, USA

[b]Biospheric Sciences Branch, NASA Goddard Space Flight Center, Greenbelt, MD 20771, USA

[c]Remote Sensing Division, Naval Research Laboratory, Washington, DC 20375, USA

[d]Earth Resources Technology, Inc., Annapolis Junction, MD 20701, USA

Corresponding author:

Qingyuan Zhang

Address:

Biospheric Sciences Branch, Code 614.4,
NASA Goddard Space Flight Center,
Greenbelt, Maryland 20771, USA

Tel: 301-614-6672

Email: qyz72@yahoo.com

Abstract – **This study presents development of prototype products for terrestrial ecosystems in preparation for the future imaging spectrometer planned for the Hyperspectral Infrared Imager (HyspIRI) mission. We present a successful demonstration example in a coniferous forest of two product prototypes: fraction of photosynthetic active radiation (PAR) absorbed by chlorophyll of a canopy ($fAPAR_{chl}$) and leaf water content (LWC), for future HyspIRI implementation at 60 m spatial resolution. For this, we used existing 30 m resolution imaging spectrometer data available from the Earth Observing One (EO-1) Hyperion satellite to simulate and prototype the level one radiometrically corrected radiance (L1R) images expected from the HyspIRI visible through shortwave infrared spectrometer. The HyspIRI-like images were atmospherically corrected to obtain surface reflectance, and spectrally resampled to produce 60 m reflectance images for wavelength regions that were comparable to all seven of the MODerate resolution Imaging Spectroradiometer (MODIS) land bands. Thus, we developed MODIS-like surface reflectance in seven spectral bands at the HyspIRI-like spatial scale, which was utilized to derive $fAPAR_{chl}$ and LWC with a coupled canopy-leaf radiative transfer model (PROSAIL2) for the coniferous forest[1]. With this study, we provide additional evidence that the $fAPAR_{chl}$ product is more realistic for describing the physiologically active canopy than the traditional fAPAR parameter for the whole canopy ($fAPAR_{canopy}$), and thus should replace it in ecosystem process models to reduce uncertainties in terrestrial carbon cycle studies and ecosystem studies.**

Index Terms – **$fAPAR_{chl}$, $fAPAR_{canopy}$, leaf water content (LWC), terrestrial carbon cycle, foliar moisture content, EO-1 Hyperion, HyspIRI**

1. INTRODUCTION

A Hyperspectral Infrared Imager (HyspIRI) mission was described by the National Research Council in its Decadal Survey Report (http://www.nap.edu/catalog.php?record_id=11820) to address terrestrial ecosystem science, as one of the next

generation NASA satellite missions. The HyspIRI mission is envisioned to carry two spectral instruments, both with ground spatial resolutions of 60 m -- a visible to shortwave infrared (VSWIR) continuous spectrum hyperspectral imager (10 nm spectral sampling) and a multi-channel thermal infrared (TIR) imager. The Earth Observing One (EO-1) Hyperion (launched in November 2000) is still operating and serves as the heritage satellite instrument for HyspIRI's VSWIR spectrometer, but it only captures 7.5 km wide ground strips, and its 30 m resolution images are acquired through user/system requests. In contrast, HyspIRI will be a global survey mission and its VSWIR instrument will have 60 m pixels across a 150 km wide ground swath, collected on an equatorial 19 day repeat cycle. Consequently, existing Hyperion data provide an excellent tool for product development in anticipation of the HyspIRI and other spaceborne imaging spectrometer missions.

The absorbed photosynthetically active radiation (APAR) fraction for a whole vegetation canopy ($fAPAR_{canopy}$, also denoted as FAPAR or FPAR[2-4]) (see Appendix A for equations) is an essential climate variable ([5-8]) needed to estimate and monitor vegetation productivity on a global basis. However, $fAPAR_{canopy}$ includes both photosynthetic and non-photosynthetic components, and has not provided consistent relationships to photosynthetic processes at the ecosystem scale [1, 9-11]. This is because the APAR available to support vegetation photosynthesis ($APAR_{PSN}$) is typically overestimated by $fAPAR_{canopy}$. However, the APAR fraction associated with the chlorophyll-containing component ($fAPAR_{chl}$, equation A.3 in Appendix A) consistently and correctly represents the physiologically active photosynthetic sector of the canopy under optimal (e.g., fully green) and less optimal (e.g., mixtures of green and senescent

vegetation) conditions affecting physiological responses. In other words, $fAPAR_{PSN}$ = $fAPAR_{chl}$ [1].

We recently demonstrated that $fAPAR_{chl}$ is superior to the use of $fAPAR_{canopy}$ in model simulations with gross primary production (GPP) or gross ecosystem production (GEP) to estimate light use efficiency (LUE), defined as $GPP/APAR_{PSN}$ [1]. The $fAPAR_{chl}$ retrievals were estimated from space for a deciduous aspen forest using five of the seven MODerate Resolution Imaging Spectroradiometer (MODIS) spectral land bands from Collection 4 daily products, for which product quality was insufficient for our model retrievals in two land bands (B3, blue; B7, $SWIR_2$). Those earlier results were indirectly validated by comparing LUE measured *in situ* at the tower (LUE_{tower}) to the LUE determined from our remote sensing/modeling approach for the forest's chlorophyll component (LUE_{chl}= $GPP/APAR_{chl}$, where $APAR_{chl}$=$fAPAR_{chl}$ *PAR). LUE_{chl} matched well with LUE_{tower} while the widely used LUE describing the whole canopy (LUE_{canopy}=$GPP/APAR_{canopy}$, where $APAR_{canopy}$= $fAPAR_{canopy}$*PAR) did not. Therefore, we recommended that $fAPAR_{chl}$ should replace $fAPAR_{canopy}$ to estimate canopy parameters related to photosynthesis for climate models and land-atmosphere interaction models [5, 7]. But further evidence should be pursued.

The spectral range for both the EO-1 Hyperion and the future HyspIRI VSWIR imaging spectrometers is between 0.4 – 2.5 μm, which spans the spectral range of the MODIS 1 – 7 land bands. In the present study, the $fAPAR_{chl}$ algorithm that was previously developed to ingest five MODIS bands was modified to utilize all seven MODIS land bands from the more radiometrically rigorous Collection 5 products. We wish to know how inclusion of these additional bands and higher spatial resolution

satellite observations (60 m vs. 500 m) affected and improved retrievals of $fAPAR_{chl}$ from HyspIRI-like VSWIR radiance images simulated from EO-1 Hyperion images. We also simultaneously retrieved leaf water content (LWC, equation A.4). The Normalized Difference Vegetation Index (NDVI, equation A.5) and Enhanced Vegetation Index (EVI, equation A.6) were used to estimate $fAPAR_{canopy}$ and $fAPAR_{chl}$, respectively [12-15], and the Land Surface Water Index (LSWI, equation A.7) was used to estimate foliar moisture content [14]. Note that $fAPAR_{canopy}$ is a linear function of NDVI[12].

The goal of this project was to apply the modified $fAPAR_{chl}$ and LWC algorithm to a coniferous forest in a heterogeneous landscape, to demonstrate the advantages of the revised algorithm to observations with spectral bands spanning the full optical spectrum at much high spatial resolution than is possible with MODIS. Our specific objectives were to test the hypotheses that: (1) $fAPAR_{chl}$ and LWC provide unique information, as compared to existing indices such as EVI, $fAPAR_{canopy}$ (linear function of NDVI), and LSWI, and (2) $fAPAR_{chl}$ and LWC retrievals benefit from higher spatial resolution and additional spectral band inputs. We begin by describing the approach to obtaining prototype HyspIRI VSWIR radiance images and then describe the modification of the $fAPAR_{chl}$-LWC algorithm from 5-band to 7-band versions. Next, we present the HyspIRI outputs of the 7-band algorithm and comparisons of our model retrievals for 500 m vs. 60 m pixels, and comparison of 500m retrievals using 5 vs. 7 spectral bands, followed by the summary conclusions.

2. METHODS

2.1 Satellite Image Pre-Processing

2.1.1 Spatially scaling up the EO-1 Hyperion radiance images to 60 m

The EO-1 Hyperion images have a spatial resolution of 30 m. We spatially scaled up the Hyperion Level One radiometrically corrected Radiance (L1R) data to 60 m by averaging Hyperion 30 m pixels in four pixel blocks [16, 17] to obtain a spatially relevant prototype of 60 m HyspIRI L1R data, and also achieving an average signal to noise response comparable to that expected for HyspIRI (≥400:1). These measured radiances were divided by solar irradiances above the atmosphere to obtain the apparent Top-of-Atmosphere (TOA) reflectances.

2.1.2. Atmospheric Correction with the ATmosphere REMoval Routine (ATREM)

In order to use spectral imaging data for quantitative remote sensing of land surfaces, the absorption and scattering effects of atmospheric gases and aerosols must be removed [18]. The HyspIRI-like L1R images (at 60 m) were atmospherically corrected using an updated version of the ATmosphere REMoval Algorithm (ATREM) with which a line-by-line model was used to calculate atmospheric gaseous transmittances [19, 20]. The surface reflectances were derived from the apparent TOA reflectances using the simulated atmospheric gaseous transmittances and the simulated molecular and aerosol scattering data. During retrievals, the integrated water vapor amount on a pixel by pixel basis can be directly derived from the 0.94 μm and the 1.14 μm atmospheric water vapor absorption features, a special advantage conveyed by continuous spectrometer data. The transmission spectrum of water vapor (H_2O), carbon dioxide (CO_2), ozone (O_3), nitrous oxide (N_2O), carbon monoxide (CO), methane (CH_4), and oxygen (O_2) in the 0.4–2.5 μm region was simulated based on the derived water vapor value, the solar and the

observational geometry, and through use of narrow band spectral models. However, the scattering effect due to atmospheric molecules and aerosols was determined with the 6S computer code [21].

2.1.3. Spectrally combining HyspIRI-like surface reflectance bands to simulate the MODIS bands 1 – 7

After obtaining atmospherically corrected HyspIRI-like 60 m surface reflectance images, the spectral values were averaged across 3-6 contiguous 10 nm Hyperion bands within the defined MODIS band ranges (Table 1) using spectral response functions to obtain reflectances spectrally comparable to those from MODIS ([22]). This yielded an image that was spatially-HyspIRI-like but spectrally-MODIS-like. To summarize, spatially scaling-up from 30 m to 60 m was performed on the Hyperion L1R radiance image, after which the ATREM atmospheric correction was performed on the 60 m HyspIRI-like L1R radiance image (60 x 60 HyspIRI pixel block) to obtain a 60 m HyspIRI-like surface reflectance image, followed by spectral averaging to obtain surface reflectance in each of the seven MODIS-like bands (Tab 1).

The vegetation canopy parameters derived from the $fAPAR_{chl}$ algorithm [1] included: leaf internal structure (N), leaf dry matter (C_m), leaf water thickness (C_w), and leaf pigment content (C_{ab}). In preliminary model runs, all seven (of 36) MODIS land bands (1-7) were found to be sensitive to N and C_m, whereas bands 1, 3 and 4 were sensitive to C_{ab}, and bands 5, 6 and 7 were sensitive to C_w [23].

Table 1. The spectral ranges covered by the MODIS and Hyperion/HyspIRI bands.

Spectral range/ Band Width	MODIS band #	Hyperion/HyspIRI band #

459 – 479 nm/ 20 nm	3 (blue)	11 – 13
545 – 565 nm/ 20 nm	4 (green)	20 – 22
620 – 670 nm/ 50 nm	1 (red)	27 – 32
841 – 875 nm/ 34 nm	2 (NIR_1)	49 – 52
1230 – 1250 nm/ 20 nm	5 (NIR_2)	108 – 111
1628 – 1652 nm/ 24 nm	6 ($SWIR_1$)	148 – 150
2105 – 2155 nm/ 50 nm	7 ($SWIR_2$)	195 – 200

2.2. Algorithm to derive $fAPAR_{chl}$ and leaf water content (LWC) using PROSAIL2 and the Metropolis approach

A complete description of the PROSAIL2 model and Metropolis approach, as applied to five spectral MODIS land bands, is given in a recent publication [1]. The coupled canopy-leaf radiative transfer model utilized in this PROSAIL2 algorithm is based on the SAIL2 canopy radiative transfer model and the PROSPECT leaf radiative transfer model. Here, we provide an overview and highlight the changes introduced in the revised approach. Additional details and information are provided in Appendix A.

In brief, a vegetation canopy can be partitioned into leaf and non-leaf (referred to as stem) components. A leaf can be further partitioned into chlorophyll, non-photosynthetic pigments (referred to as brown pigment, C_{brown}), water and dry matter. The PROSAIL2 model has fourteen biophysical and biochemical variables (See Appendix A), five leaf variables that simulate leaf optical properties (N, C_{ab}, C_m, C_w, C_{brown}), a soil/litter variable that simulates soil/litter optical properties ($SOIL_A$), and a variable that simulates stem optical properties ($STEM_A$).

We modified the previous MODIS $fAPAR_{chl}$ algorithm [1] by replacing the 5-band likelihood function with that for 7-band surface reflectances obtained from section

2.1.3 (Eqns. 1 & 2). The Markov Chain Monte Carlo (MCMC) method (Metropolis) is employed for inversion. This method assumes that the observed spectral reflectances $X_i = \left[x_{i1}, \cdots, x_{ip}\right]$ (p=7, Tab. 1) differ from the model predicted values $U_i = \left[u_{i1}, \cdots, u_{ip}\right]$ according to a mean zero p-variate Gaussian error model that results in the likelihood function:

$$L = \prod_{i=1}^{n} \frac{1}{\left(\sqrt{2\pi}\right)^{p} \left|\sum\right|^{1/2}} e^{-(X_i - U_i)' \Sigma^{-1} (X_i - U_i)/2}, \qquad (1)$$

where *n* is the number of data points sampled according to Eqn. 8 of Zhang et al. [1] and Σ is the variance-covariance matrix of X:

$$\Sigma_e = \left(s_{ij}\right)_{p \times p} \qquad i, j = 1, \square, p \qquad (2)$$
$$s_{ij} = \frac{1}{n} \sum_{k=1}^{n} (x_{ki} - u_{ki})(x_{kj} - u_{kj})$$

The new 7-band $fAPAR_{chl}$ algorithm provides simultaneous solutions for C_w and C_m, enabling the solution of LWC (see equation A.4). The full solution of the fourteen parameters is a statistical posterior distribution based on the radiative transfer model and the remote sensing observation (see section 2.1.3).

The fourteen parameters and the derived $fAPAR_{chl}$ and LWC may be grouped into three classes based on their posterior statistical distributions: well-constrained, edge-hitting and poorly-constrained. The posterior statistical distributions can provide the mode(s) of the fourteen variables, $fAPAR_{chl}$ and LWC (if they exist) (please see Zhang et al. [24] for details). A mode for a variable is one "traditional" (best) point solution, i.e., the most likely value of the variable to fit both the PROSAIL2 model and the remote sensing observation. From the case study of this paper (see section 2.3 for site description), we discovered that there was one and only one mode for $fAPAR_{chl}$ and for

LWC per satellite observation. The reason is that chlorophyll, leaf water and dry matter have unique spectral characteristics, respectively. These components can be distinguished using spectral information of the seven bands, and will not mess up with each other or other components of a canopy.

The EVI [25], NDVI [26], $fAPAR_{canopy}$, and LSWI [14] were also calculated (see Appendix A for equations), and compared with results for $fAPAR_{chl}$ or LWC, as appropriate, at both MODIS (500 m) and HyspIRI (60 m) spatial resolutions. We also calculated $fAPAR_{canopy}$ for the whole canopy, based on a widely-used formula which relates $fAPAR_{canopy}$ and NDVI (e.g., [12, 13, 15]):

$$fAPAR_{canopy} = 1.24 \times NDVI - 0.168 \quad (3)$$

We also utilized the same 7-band approach (Eqns. 1 & 2) to retrieve $fAPAR_{chl}$ and LWC from MOD09A1 (the 8-day composite reflectance MODIS product (M)) acquired on day 185 (July 3), 2008, which was close to the acquisition date of the original Hyperion image (June 28, 2008). This enabled us to compare the 60 m HyspIRI-like product (H) with MODIS 500 m product.

2.3. Study Site

The study site (Figure 1) was a Douglas fir forest surrounding an instrumented tower (hereafter DF49: 49°52’ N, 125° 20’W, 300 m elevation) in the Canadian Carbon Program (CCP) network. The DF49 is located on the eastern side of Vancouver Island, British Columbia, Canada, and the forest stand around the tower (indicated by a circle in Fig. 1) is mainly comprised of Douglas fir with some western red cedar, and western hemlock [27]. The study area was a 120 x 120 grid formed by Hyperion pixels at the

original 30 m spatial resolution around the DF49 site. A true color RGB image at the 60 m HyspIRI pixel spatial resolution (Fig. 1) can be compared with the land cover map produced using the ISODATA method of ENVI (Figure 2), which utilized the surface reflectances of the original HyspIRI bands (Tab. 1) for land cover classification. "Un-vegetated" areas are associated with roads or sparse vegetation. Harvested areas show various stages of forest regeneration. Wetter forested areas are dominated by hemlock, alder and maple (personal communication, Nicholas Coops, Univ. BC).

3. RESULTS

3.1. HyspIRI-Like Results

Here, we present the results of the revised 7-band $fAPAR_{chl}$-LWC algorithm (described in Section 2.2) applied to the mid-summer HyspIRI-like L1R radiance image in the vicinity of the DF49 Douglas fir tower site (described in section 2.3) for the purpose of developing and evaluating prototype products.

Fig. 3 has three sub-figures for our study site showing the spatial distributions for three of the variables of interest: (a) $fAPAR_{chl}$; (b) $fAPAR_{canopy}$ (based on NDVI using Eqn. 3); and (c) EVI, all presented on the same relative scale between 0.0 and 1.0. Clearly, the values in the $fAPAR_{chl}$ map are substantially and statistically lower than those exhibited by the $fAPAR_{canopy}$ map. Table 2 lists the mode, mean and median values computed for the study area shown in Figs. 1b, 2, and 3a-c for $fAPAR_{chl}$, EVI, $fAPAR_{canopy}$, and NDVI. These statistical values reveal that $fAPAR_{chl}$ and EVI provide substantially lower values than NDVI and $fAPAR_{canopy}$.

The vegetation photosynthesis model (VPM[14]) assumes $fAPAR_{chl}$ = EVI, but we find that this assumption is not always correct. And, overestimates of $APAR_{PSN}$ result if we assume $fAPAR_{chl}$ = $fAPAR_{canopy}$.

Table 2. The values of mode(s), mean and median of the $fAPAR_{chl}$, EVI, $fAPAR_{canopy}$, and NDVI values for area shown in Figure 3. Number of HyspIRI-like Pixels = 3600

	mode(s)	mean	median
$fAPAR_{chl}$	0.559, 0.714	0.520	0.544
EVI	0.437	0.460	0.452
$fAPAR_{canopy}$	0.893	0.824	0.870
NDVI **	0.855	0.800	0.837

** map not shown.

The LWC and LSWI maps are shown in Figure 4. LWC values of wetter forest areas (0.600 – 0.909) differ substantially from LSWI values (0.202 – 0.483). Although the LSWI has been shown to represent water status of vegetation in some studies [14, 28], this index cannot distinguish canopy water from background water (e.g., soil water). The LWC of different plant species among land cover types might vary, as shown in Fig. 4(a) for the LWC dynamics per class. The broad-leaf deciduous leaves in the wetter forest areas had higher average LWC than the Douglas fir leaves (Fig. 4a).

The histograms for $fAPAR_{chl}$, $fAPAR_{canopy}$, and EVI and the histograms for LWC and LSWI are shown in Figures 5 and 6, respectively. Peak frequencies occurred at very different values: $fAPAR_{chl}$ (0.559), EVI (0.437), and $fAPAR_{canopy}$ (0.893); but peak frequencies for LWC and LSWI occurred at similar value (~0.49). The $fAPAR_{chl}$

parameter displayed minor mode at 0.714. For forests, the magnitude is higher and the range is wider for $fAPAR_{chl}$ as compared to EVI (Fig. 3a,c).The frequency of the mode derived from the HyspIRI-like LWC map is about three times that of the comparable mode for the LSWI (Fig. 6). Scatter plot comparisons are also shown for these pairs: $fAPAR_{chl}$ vs. $fAPAR_{canopy}$; $fAPAR_{chl}$ vs. EVI; and LWC vs. LSWI (Figure 7). The first pair exhibits that $fAPAR_{canopy}$ is greater than $fAPAR_{chl,}$. While values are closer between EVI and $fAPAR_{chl\ ,}$ the slope relating these two variables clearly deviates from the 1:1 line. No apparent correlation is seen for the third pair (LWC and LSWI). LSWI cannot be used to replace or predict LWC well, as demonstrated in Fig. 7c.

The pixels classified as "unvegetated" were recently harvested (personal communication, Nicholas Coops, Univ. BC). The $fAPAR_{chl}$ values for those pixels are close to zero, as should be expected for areas without green vegetation. That is to say, $fAPAR_{chl}$ has a physical and physiological meaning. However the NDVI and EVI values of those pixels, which are greater than 0.4 and 0.2, respectively, indicate the presence of some green vegetation. NDVI (and the derived parameter, $fAPAR_{canopy}$) saturate for pixels with leaf area index (LAI) greater than 3 [25] while $fAPAR_{chl}$ does not.

3.2. Comparing HyspIRI-Like and MODIS Parameter Estimates

From the processed MODIS image (July 3, 2008, DOY 185), we selected the pixel that covers the DF49 site. The HyspIRI-like maps have considerably more spatial details than those based on the MODIS image. To compare our retrievals from HyspIRI-like images with those based on the MODIS image, using the same 7-band approach

(Eqns. 1 & 2), we chose only the HyspIRI pixels that fall within 240 m of the DF49 tower site. Forty-nine HyspIRI pixels were selected (Tab. 3).

Table 3. Comparison at the DF49 tower site of the $fAPAR_{chl}$, $fAPAR_{canopy}$,NDVI, EVI, LSWI, and LWC values from the simulated HyspIRI-like (60 m) image, with the MODIS image (500 m), and published field measurements (H: HyspIRI-like data, M: 7-band MODIS based data).

	Parameters		Value (± STDEV)	Sample size, Comments
fAPAR related parameters	$fAPAR_{chl}$	H	0.583 ± 0.038	n = 49 pixels
		M	0.533	single pixel value
	$fAPAR_{canopy}$	H	0.907 ± 0.006	n = 49 pixels
		M	0.949	single pixel value
		Tower based	0.94	Hember et al. (2010) day 180-185 of 2008
	NDVI	H	0.867 ± 0.005	n = 49 pixels
		M	0.901	single pixel value
	EVI	H	0.449 ±0.017	n = 49 pixels
		M	0.445	single pixel value
	$fAPAR_{green-leaf}$	Tower based	0.79	Hilker et al. (2010) day 180-185 of 2008
Leaf water related parameters	LWC	H	0.494 ± 0.008	n = 49 pixels
		M	0.493	single pixel value
		Field	0.44 – 0.67	Agee et al. (2002),

		measurements		Keyes (2006) growing season of multi years
	LSWI	H	0.506 ± 0.013	n = 49 pixels
		M	0.510	single pixel value

In the comparison of the 7-band HyspIRI-like (H) and true MODIS (M) products (Tab. 3), the mean $fAPAR_{chl}$ values (H) and the single MODIS $fAPAR_{chl}$ value (M) were fairly similar . The mean H and M satellite values for $fAPAR_{canopy}$ were comparable to the tower based canopy-level fAPAR (0.94 [29]) determined from the DF49 tower radiation measurements for the same period. The green leaf fAPAR (0.79 [30]) estimated using the approach developed by Chen et al. (1996 and 2006) [31, 32] represented the combined effects of chlorophyll fAPAR, and the fAPAR of leaf dry matter and brown pigments of the canopy for the same period. Thus, the green leaf fAPAR was intermediate between estimates for $fAPAR_{chl}$ and $fAPAR_{canopy}$.

LWC provides quantitative information on foliar moisture content. It is not only a critical indicator of vegetation growth status, but also an important factor in the canopy susceptibility to the fire ignition process. Our retrievals for H and M (Tab. 3) both fall within the published Douglas fir LWC range (between 0.67 and 0.44), which includes both young and old leaves [33, 34]. The mean LWC value for the forty-nine HyspIRI-like pixels (Fig. 4a) is the same as that for the MODIS single pixel LWC (~0.49, Tab. 3).

In addition to application of the 7-band algorithm to the MODIS pixel that covers the DF49 site, we also calculated $fAPAR_{chl}$ and LWC using the original 5-band algorithm [1]. The 7-band vs. 5-band $fAPAR_{chl}$ histograms of the pixel have the same mode value (0.533), with only slightly different standard deviations (0.071 vs. 0.072).However, while

the 7-band vs. 5-band LWC histograms at the tower site have the same mode value, their standard deviations differ (0.169 vs. 0.174), such that less uncertainty is incurred using the 7-band version.

4. DISCUSSION

This study describes how to estimate two products ($fAPAR_{chl}$ & LWC) for HyspIRI L1R radiance and presents some initial prototype results. In addition to our primary products ($fAPAR_{chl}$ and LWC), we also determined values and map products for the EVI, $fAPAR_{canopy}$, and LSWI. Although $fAPAR_{chl}$ and EVI were the most similar, the range of values and the modes for $fAPAR_{chl}$ were larger than those obtained for the EVI (Fig. 5a, c; Tab. 2). Likewise, the dynamic range for $fAPAR_{canopy}$, was smaller than the range for $fAPAR_{chl}$ values (Fig. 5a,b). When comparing $fAPAR_{chl}$ and EVI, we found that when $fAPAR_{chl} = 0.5$, the EVI range is 0.384 – 0.533; but when EVI = 0.5, the $fAPAR_{chl}$ range is 0.410 – 0.686 (Fig. 7b).

In addition to better spatial detail, one advantage of the 7-band $fAPAR_{chl}$ & LWC algorithm is that it does not need land cover type information as an input to run the model inversion, whereas the MODIS standard $fAPAR_{canopy}$ (i.e., FPAR) product does. The 7-band algorithm can provide $fAPAR_{chl}$ and LWC products with less uncertainty (e.g., smaller standard deviations), as compared to results obtained with the previous 5-band algorithm, even for a relatively homogeneous forest area (circle in Fig. 1 (b)). The outputs of the algorithm ($fAPAR_{chl}$ and LWC) can be used for seasonal analysis, interannual analysis, phenological study, and land use and land cover change research -- including disturbance studies and disaster monitoring (e.g., fire, drought and flooding).

Our study also demonstrates the flexibility that an imaging spectrometer allows for inter-instrument comparisons.

The remote sensing community uses three groups of inversion strategies: MCMC approaches, look-up-tables, and gradient-based approaches. With the Metropolis approach (a MCMC method), we can globally search for the optimal solution, a posterior distribution. However, look-up-table methods provide fixed step lengths for all parameters before inversion, whereas gradient-based methods can only search local optima and rely on initial guesses. We anticipate that application of our algorithm to satellite images will be useful for the current and future national and international research projects that rely on remotely sensed data, including the North American Carbon Program (NACP).

5. CONCLUSION

We successfully demonstrated here that the two products ($fAPAR_{chl}$ and LWC) provide unique information. The most important finding in this study is that $fAPAR_{chl}$ values differ from those for EVI, NDVI and $fAPAR_{canopy}$ in most cases. EVI does not always equal to $fAPAR_{chl}$. We also find that: $fAPAR_{chl} \neq fAPAR_{canopy}$ (or NDVI); and LWC ≠ LSWI. In other words, we reject the null hypotheses that equate the EVI and $fAPAR_{canopy}$ with $fAPAR_{chl}$, or LSWI with LWC. HyspIRI also has the potential to provide the spatial variance of the two products that can't be extracted from MODIS. We realize that real HyspIRI images, or those of another future imaging spectrometer, will differ in some ways from Hyperion, which can be taken into account with the at-launch version of the algorithm.

ACKNOWLEDGMENTS

Four anonymous reviewers have provided helpful suggestion and comments for the manuscript. This study was supported by two NASA Headquarters sponsored programs, the Earth Observing One (EO-1) Mission Science Office (Sponsor, Garik Gutman) and the HyspIRI science support project at the Goddard Space Flight Center (NASA/GSFC), through William (Woody) Turner.

Appendix A

In brief, a vegetation canopy can be partitioned into leaf and non-leaf (hereafter referred to as stem) components. A leaf can be further partitioned into chlorophyll, non-photosynthetic pigments (hereafter referred to as brown pigment, C_{brown}), water and dry matter (or C_{ab}, C_{brown}, C_w, C_m). The PROSAIL2 model has fourteen biophysical and biochemical variables: plant area index (PAI), stem fraction (SFRAC), cover fraction (CF), stem inclination angle (STINC), stem BRDF effect variable (STHOT), leaf inclination angle (LFINC), leaf BRDF effect variable (LFHOT), five leaf variables that simulate leaf optical properties (N, C_{ab}, C_m, C_w, C_{brown}), one soil/litter variable that simulates soil/litter optical properties ($SOIL_A$), and one variable that simulates stem optical properties ($STEM_A$). The Markov Chain Monte Carlo (MCMC) method (Methopolis) is employed for inversion.

One can calculate $fAPAR_{canopy}$ [12] and $fAPAR_{chl}$ [1] with equations:

$$APAR_{canopy} = APAR_{chl} + APAR_{dry\ matter} + APAR_{brown\ pigment} + APAR_{stem} \qquad (A.1)$$

$$fAPAR_{canopy} = \frac{APAR_{canopy}}{PAR_0} \quad \text{(A.2)}$$

$$fAPAR_{chl} = \frac{APAR_{chl}}{PAR_0} \quad \text{(A.3)}$$

where PAR_0 is the incoming PAR at the top of the canopy, and $APAR_{canopy}$, $APAR_{chl}$, $APAR_{dry\ matter}$, $APAR_{brown\ pigment}$, and $APAR_{stem}$ are absorbed PAR by canopy, chlorophyll in leaf, dry matter in leaf, brown pigment in leaf, and stem, respectively. One has to know the value of PAR_0 and the values of the fourteen parameters to calculate $APAR_{chl}$ and $APAR_{canopy}$ in equation A.1. One may assume PAR_0 be any positive value to calculate $fAPAR_{chl}$ and $fAPAR_{canopy}$ because they are ratios (equations A.2 and A.3). We present NDVI based $fAPAR_{canopy}$ for this study because of the linear relationship between $fAPAR_{canopy}$ and NDVI (Eqn. 3), which is based on the simulation study using the SAIL[12].

The leaf water thickness (C_w, g/cm^2 or cm) and leaf dry matter (C_m, g/cm^2) are two of the fourteen parameters of PROSAIL2, and the inversion algorithm provides their posterior distributions as outputs. Leaf water content (LWC) is defined as the fraction of leaf water weight to fresh leaf weight[35]. That is to say,

$$LWC = \frac{C_W}{C_W + C_m} \quad \text{(A.4)}$$

EVI [25], NDVI [26], and LSWI [14] are also calculated:

$$EVI = 2.5 \times \frac{\rho_{NIR_1} - \rho_{red}}{\rho_{NIR_1} + 6.0 \times \rho_{red} - 7.5 \times \rho_{blue} + 1.0} \quad \text{(A.5)}$$

$$NDVI = \frac{\rho_{NIR_1} - \rho_{red}}{\rho_{NIR_1} + \rho_{red}} \quad \text{(A.6)}$$

$$LSWI = \frac{\rho_{NIR_1} - \rho_{SWIR_1}}{\rho_{NIR_1} + \rho_{SWIR_1}} \quad \text{(A.7)}$$

where ρ is reflectance.

REFERENCES

[1] Q. Zhang, E. M. Middleton, H. A. Margolis, G. G. Drolet, A. A. Barr, and T. A. Black, "Can a MODIS-derived estimate of the fraction of PAR absorbed by chlorophyll (FAPARchl) improve predictions of light-use efficiency and ecosystem photosynthesis for a boreal aspen forest?," *Remote Sensing of Environment,* vol. 113, pp. 880-888, April 15, 2009.

[2] J. S. Kimball, L. A. Jones, K. Zhang, F. A. Heinsch, K. C. McDonald, and W. C. Oechel, "A Satellite Approach to Estimate Land–Atmosphere CO2 Exchange for Boreal and Arctic Biomes Using MODIS and AMSR-E," *IEEE Transactions on Geoscience and Remote Sensing,* vol. 47, pp. 569-587, 2009.

[3] X. Xiao, "Light Absorption by Leaf Chlorophyll and Maximum Light Use Efficiency," *IEEE Transactions on Geoscience and Remote Sensing,* vol. 44, pp. 1933-1935, July 2006.

[4] F. A. Heinsch, M. Zhao, S. W. Running, J. S. Kimball, R. R. Nemani, K. J. Davis, P. V. Bolstad, B. D. Cook, A. R. Desai, D. M. Ricciuto, B. E. Law, W. C. Oechel, H. Kwon, H. Luo, S. C. Wofsy, A. L. Dunn, J. W. Munger, D. D. Baldocchi, L. Xu, D. Y. Hollinger, A. D. Richardson, P. C. Stoy, M. B. S. Siqueira, R. K. Monson, S. P. Burns, and L. B. Flanagan, "Evaluation of Remote Sensing Based Terrestrial Productivity From MODIS Using Regional Tower Eddy Flux Network Observations," *IEEE Transactions on Geoscience and Remote Sensing,* vol. 44, pp. 1908-1925, 2006.

[5] P. J. Sellers, D. A. Randall, G. J. Collatz, J. A. Berry, C. B. Field, D. A. Dazlich, C. Zhang, G. D. Collelo, and L. Bounoua, "A revised land surface parameterization (SiB2) for atmospheric GCMs .I: Model formulation," *Journal of Climate,* vol. 9, pp. 676-705, APR 1996.

[6] R. H. Waring, N. C. Coops, and J. J. Landsberg, "Improving predictions of forest growth using the 3-PGS model with observations made by remote sensing," *Forest Ecology and Management,* vol. 259, pp. 1722–1729, 2010.

[7] P. J. Sellers, S. O. Los, C. J. Tucker, C. O. Justice, D. A. Dazlich, G. J. Collatz, and D. A. Randall, "A revised land surface parameterization (SiB2) for atmospheric GCMs .II: The generation of global fields of terrestrial biophysical parameters from satellite data," *Journal of Climate,* vol. 9, pp. 706-737, APR 1996.

[8] R. E. Dickinson, "Applications of Terrestrial Remote Sensing to Climate Modeling," in *Advances in Land Remote Sensing,* S. Liang, Ed.: Springer, 2008.

[9] D. P. Turner, W. D. Ritts, W. B. Cohen, S. T. Gower, M. S. Zhao, S. W. Running, S. C. Wofsy, S. Urbanski, A. L. Dunn, and J. W. Munger, "Scaling Gross Primary Production (GPP) over boreal and deciduous forest landscapes in support of MODIS GPP product validation," *Remote Sensing of Environment,* vol. 88, pp. 256-270, DEC 15 2003.

[10] D. P. Turner, S. Urbanski, D. Bremer, S. C. Wofsy, T. Meyers, S. T. Gower, and M. Gregory, "A cross-biome comparison of daily light use efficiency for gross primary production," *Global Change Biology,* vol. 9, pp. 383-395, MAR 2003.

[11] D. P. Turner, W. D. Ritts, M. Zhao, S. A. Kurc, A. L. Dunn, S. Wofsy, E. Small, and S. W. Running, "Assessing Interannual Variation in MODIS-Based Estimates

of Gross Primary Production," *IEEE Computational Science & Engineering,* vol. 44, pp. 1899-1907, July 2006.

[12] S. N. Goward and K. F. Huemmrich, "Vegetation Canopy PAR Absorptance and the Normalized Difference Vegetation Index - an Assessment Using the SAIL Model," *Remote Sensing of Environment,* vol. 39, pp. 119-140, Feb 1992.

[13] D. A. Sims, A. F. Rahman, V. D. Cordova, D. D. Baldocchi, L. B. Flanagan, A. H. Goldstein, D. Y. Hollinger, L. Misson, R. K. Monson, H. P. Schmid, S. C. Wofsy, and L. K. Xu, "Midday values of gross CO2 flux and light use efficiency during satellite overpasses can be used to directly estimate eight-day mean flux," *Agricultural and Forest Meteorology,* vol. 131, pp. 1-12, 2005.

[14] X. M. Xiao, Q. Y. Zhang, B. Braswell, S. Urbanski, S. Boles, S. Wofsy, B. Moore, and D. Ojima, "Modeling gross primary production of temperate deciduous broadleaf forest using satellite images and climate data," *Remote Sensing of Environment,* vol. 91, pp. 256-270, MAY 30 2004.

[15] C. O. Justice, E. Vermote, J. R. G. Townshend, R. Defries, D. P. Roy, D. K. Hall, V. V. Salomonson, J. L. Privette, G. Riggs, A. Strahler, W. Lucht, R. B. Myneni, Y. Knyazikhin, S. W. Running, R. R. Nemani, Z. M. Wan, A. R. Huete, W. van Leeuwen, R. E. Wolfe, L. Giglio, J. P. Muller, P. Lewis, and M. J. Barnsley, "The Moderate Resolution Imaging Spectroradiometer (MODIS): Land Remote Sensing for Global Change Research," *IEEE Transactions on Geoscience and Remote Sensing,* vol. 36, pp. 1228-1249, Jul 1998.

[16] B. D. Cook, P. V. Bolstad, E. Næsset, R. S. Anderson, S. Garrigues, J. T. Morisette, J. Nickeson, and K. J. Davis, "Using LiDAR and quickbird data to model plant production and quantify uncertainties associated with wetland detection and land cover generalizations," *Remote Sensing of Environment,* vol. 113, pp. 2366–2379, 2009.

[17] X. M. Xiao, Q. Y. Zhang, S. Saleska, L. Hutyra, P. D. Camargo, S. Wofsy, S. Frolking, S. Boles, M. Keller, and M. B., "Satellite-based modeling of gross primary production in a seasonally moist tropical evergreen forest," *Remote Sensing of Environment,* vol. 94, pp. 105 -122, 2005.

[18] Y. J. Kaufman and D. Tanre, "Strategy for direct and indirect methods for correcting the aerosol effect on remote sensing: From AVHRR to EOS-MODIS," *Remote Sensing of Environment,* vol. 55, pp. 65-79, JAN 1996.

[19] B.-C. Gao, K. H. Heidebrecht, and A. F. H. Goetz, "Derivation of scaled surface reflectances from AVIRIS data," *Remote Sensing of Environment,* vol. 44, pp. 165 - 178, 1993.

[20] B.-C. Gao and C. O. Davis, "Development of a line-by-line-based atmosphere removal algorithm for airborne and spaceborne imaging spectrometers," *SPIE,* vol. 3118, pp. 132 - 141, 1997.

[21] E. F. Vermote, D. Tanre, J. L. Deuze, M. Herman, and J. J. Morcrette, "Second Simulation of the Satellite Signal in the Solar Spectrum, 6S: An overview," *IEEE Transactions on Geoscience and Remote Sensing,* vol. 35, pp. 675-686, May 1997.

[22] S. G. Ungar, J. S. Pearlman, J. A. Mendenhall, and D. Reuter, "Overview of the Earth Observing One (EO-1) Mission," *IEEE Transactions on Geoscience and Remote Sensing,* vol. 41, pp. 1149 - 1159, June 2003.

[23] X. Hao and J. J. Qu, "Retrieval of real-time live fuel moisture content using MODIS measurements," *Remote Sensing of Environment,* vol. 108, pp. 130-137, 2007.
[24] Q. Y. Zhang, X. M. Xiao, B. Braswell, E. Linder, F. Baret, and B. Moore, "Estimating light absorption by chlorophyll, leaf and canopy in a deciduous broadleaf forest using MODIS data and a radiative transfer model," *Remote Sensing of Environment,* vol. 99, pp. 357-371, 2005.
[25] A. R. Huete, H. Q. Liu, K. Batchily, and W. vanLeeuwen, "A comparison of vegetation indices global set of TM images for EOS-MODIS," *Remote Sensing of Environment,* vol. 59, pp. 440-451, MAR 1997.
[26] D. W. Deering, "Rangeland reflectance characteristics measured by aircraft and spacecraft sensors," in *College Station* TX: Texas A&M University, 1978, p. 338.
[27] T. Hilker, N. C. Coops, C. R. Schwalm, R. S. Jassal, T. A. Black, and P. Krishnan, "Effects of mutual shading of tree crowns on prediction of photosynthetic light-use efficiency in a coastal Douglas-fir forest," *Tree Physiology,* vol. 28, pp., 825–834, 2008.
[28] Q. Zhang, X. Xiao, B. Braswell, E. Linder, S. Ollinger, M. L. Smith, J. P. Jenkins, F. Baret, A. D. Richardson, B. Moore, and R. Minocha, "Characterization of seasonal variation of forest canopy in a temperate deciduous broadleaf forest, using daily MODIS data " *Remote Sensing of Environment,* vol. 105, pp. 189-203, 2006.
[29] R. A. Hember, N. C. Coops, T. A. Black, and R. D. Guy, "Simulating gross primary production across a chronosequence of coastal Douglas-fir forest stands with a production efficiency model," *Agricultural and Forest Meteorology,* vol. 150, pp. 238-253, 2010.
[30] T. Hilker, F. G. Hall, N. C. Coops, A. Lyapustin, Y. Wang, Z. Nesic, N. Grant, T. A. Black, M. A. Wulder, N. Kljun, C. Hopkinson, and L. Chasmer, "Remote sensing of photosynthetic light-use efficiency across two forested biomes: Spatial scaling," *Remote Sensing of Environment,* vol. 114, pp. 2863-2874, Dec 2010.
[31] J. M. Chen, "Canopy Architecture and Remote Sensing of the Fraction of Photosynthetically Active Radiation Absorbed by Boreal Conifer Forests," *IEEE Transactions on Geoscience and Remote Sensing,* vol. 34, pp. 1353-1368, Nov 1996.
[32] J. M. Chen, A. Govind, O. Sonnentag, Y. Zhang, A. Barr, and B. Amiro, "Leaf area index measurements at Fluxnet-Canada forest sites," *Agricultural and Forest Meteorology,* vol. 140, pp. 257-268, 2006.
[33] J. K. Agee, C. S. Wright, N. Williamson, and M. H. Huff, "Foliar moisture content of Pacific Northwest vegetation and its relation to wildland fire behavior," *Forest Ecology and Management,* vol. 167, pp. 57-66, 2002.
[34] C. R. Keyes, "Foliar Moisture Contents of North American Conifers," *USDA Forest Service Proceedings,* vol. RMRS, pp. 395-399, 2006.
[35] E. Garnier and G. Laurent, "Leaf anatomy, specific mass and water content in congeneric annual and perennial grass species," *New Phytologist,* vol. 128, pp. 725 - 736, 1994.

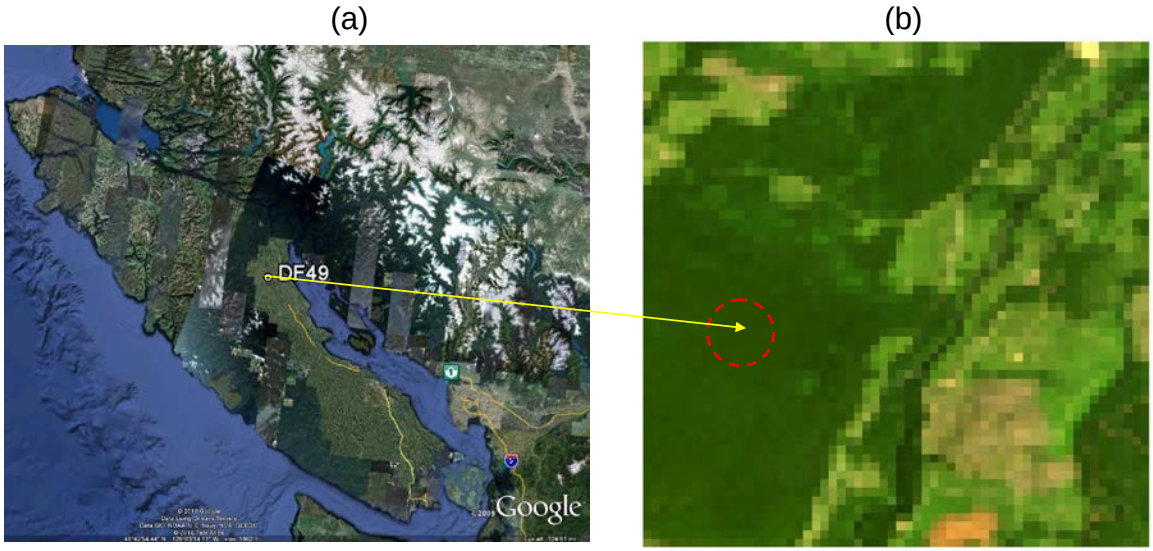

Fig. 1. (a) The location of the Douglas-fir site (DF49) on Vancouver Island, British Columbia, Canada; and (b) a true color red/green/blue (RGB) image for the DF49 area using simulated HyspIRI data on DOY 180, 2008 (June 28, 2008), where the circle designates the fetch of the DF49 flux tower.

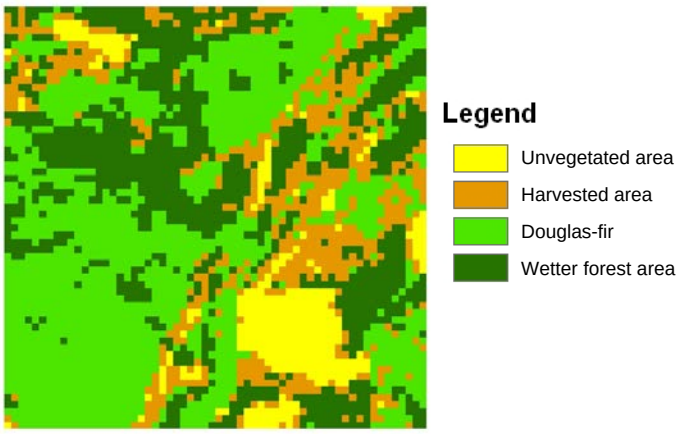

Fig. 2. Land cover map for the DF49 area using simulated HyspIRI data based on the EO-1 Hyperion image collected on DOY 180, 2008 (June 28, 2008).

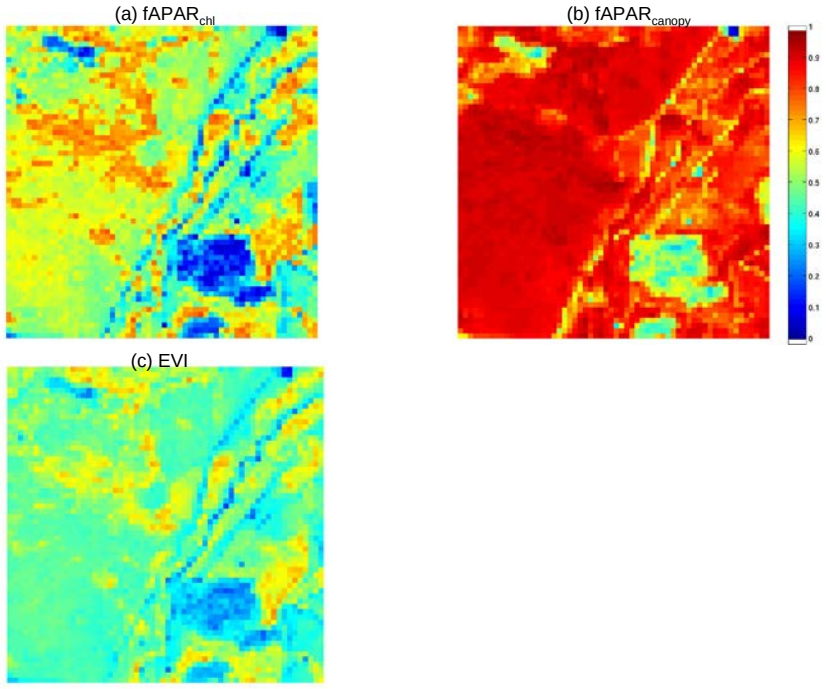

Fig. 3. HyspIRI-like maps for the DF49 area: (a) fAPAR$_{chl}$; (b) fAPAR$_{canopy}$ computed from NDVI (Eqn. 3); and (c) EVI. Data were simulated from the mid-summer Hyperion image acquired on DOY 180, 2008 (June 28, 2008).

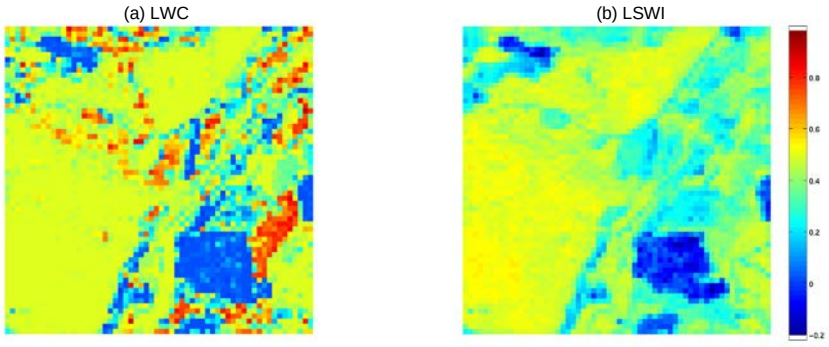

Fig. 4. HyspIRI-like maps for the DF49 area: (a) leaf water content (LWC); and (b) LSWI. Data were simulated from the mid-summer Hyperion image acquired on DOY 180, 2008 (June 28, 2008).

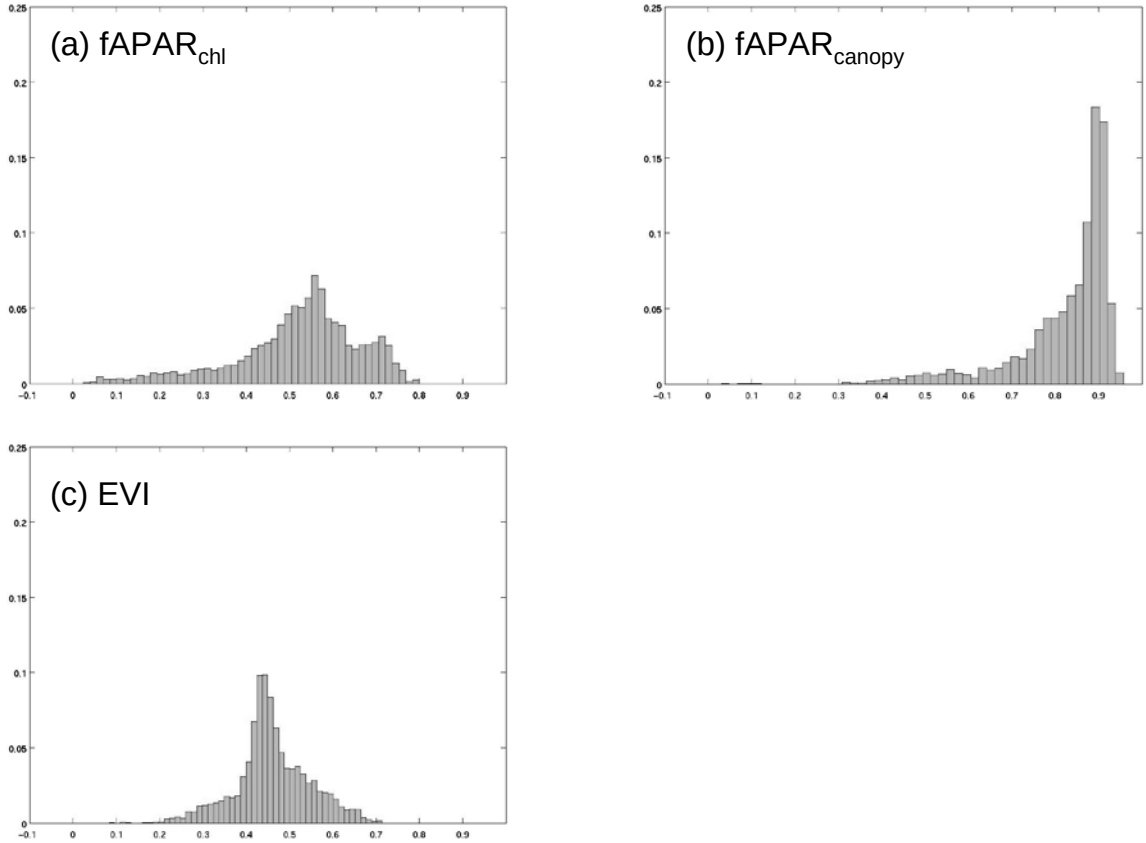

Fig. 5. Histograms for (a) fAPAR$_{chl}$; (b) fAPAR$_{canopy}$; and (c) EVI for the DF49 area shown in the Fig. 3 maps.

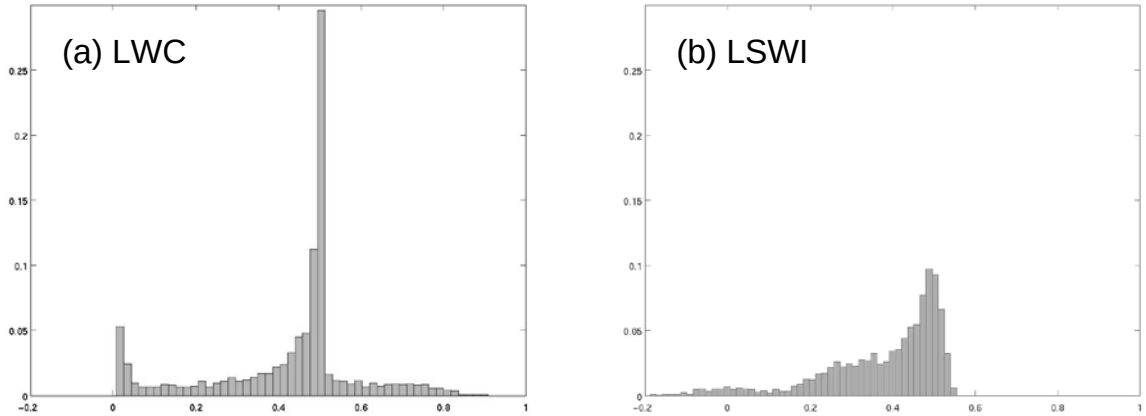

Fig. 6. Histograms for (a) LWC and (b) LSWI for the DF49 area shown in the Fig. 4 maps.

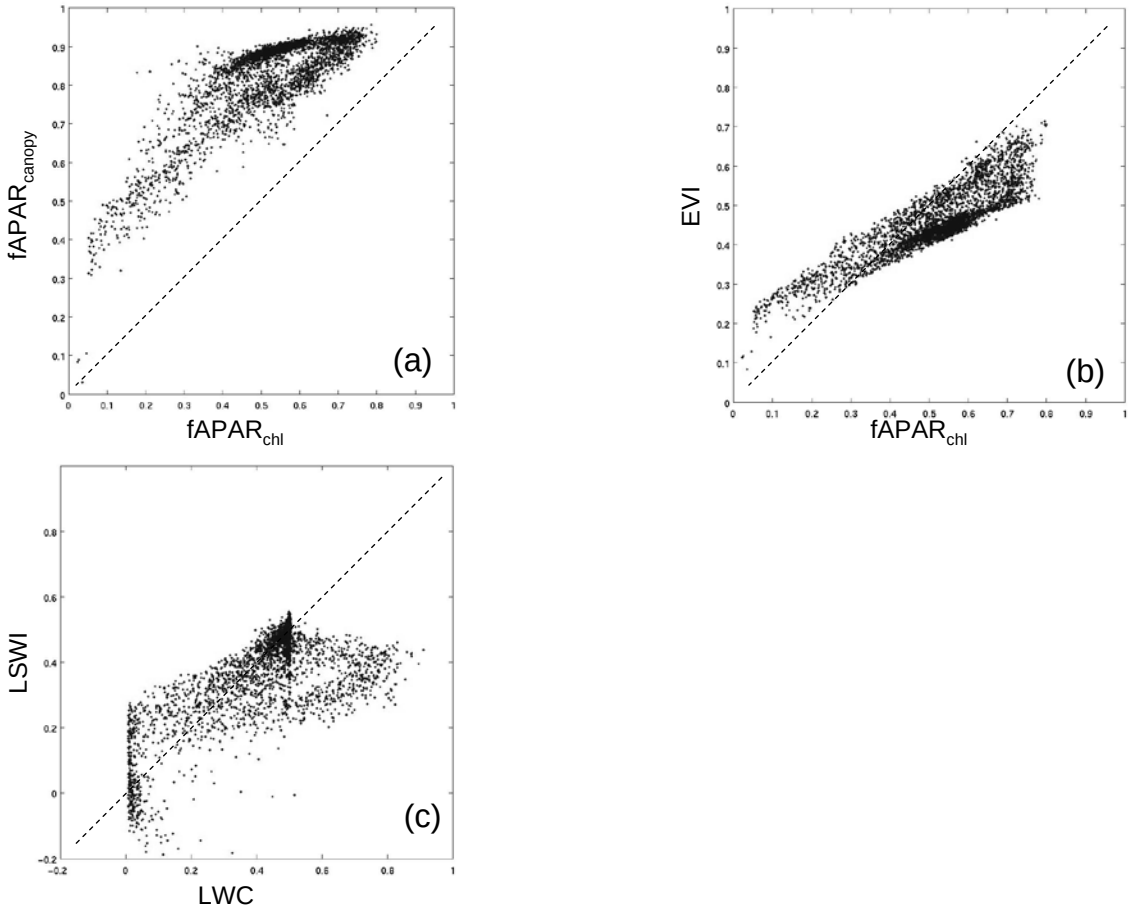

Fig. 7. Comparisons for (a) $fAPAR_{chl}$ vs. $fAPAR_{canopy}$; (b) $fAPAR_{chl}$ vs. EVI; and (c) LWC vs. LSWI. Data are derived from the simulated HyspIRI image acquired on DOY 180, 2008 (June 28, 2008).